Obtaining desired shapes of cable-driven continuum robots using general cable routing

Soumya Kanti Mahapatra[1] and Ashitava Ghosal[1⋆]

Department of Mechanical Engineering, Indian Institute of Science, Bangalore, Karnataka 560012, India
soumyam@iisc.ac.in and asitava@iisc.ac.in,

Abstract. Cable-driven continuum robots (CCR) with generally routed cables are capable of achieving complex shapes, which a straight-routed CCR with multiple sections cannot achieve. This paper presents an optimization-based algorithm that can predict a routing and the amount of cable actuation required to attain a prescribed desired final shape in a CCR. The algorithm is based on discretizing the CCR with several four-bar mechanisms and is purely geometry based. The actuation required to obtain the desired shape and to reach a desired position is a length parameter rather than a force and is easy to visualize. The results are compared with the previously known forward kinematics model and show an RMS error of less than 2% of the total CCR length.

Keywords: flexible backbone, cable-driven continuum robot, general routing, desired shapes

1 Introduction

Continuum robots have a continuous flexible structure instead of the discrete segments found in traditional robots. The main advantage of continuum robots is their inherent compliance which allows them to better adapt to complex and dynamic environments and makes them inherently safer. They also tend to be lightweight and dexterous than traditional robots, making them ideal for tasks that require flexibility. The CCR consists of a flexible backbone as the main element. This backbone can be actuated by various means [1]. Among the most widely utilized actuation methods, cable-driven continuum robots (CCR) are favored because of their ease of construction, operation, and usage. Consequently, CCRs find numerous applications in various fields [2,3], notably biomimetics, medical devices, space applications, and search and rescue operations.

A flexible rod-like member known as the *backbone* forms the main member of a CCR. Circular disks, evenly spaced along the backbone, are attached and feature holes arranged in a circular pattern around the backbone's periphery. Through these holes, thin cables are routed from the base to the tip of the CCR – Figure 1a depicts a CCR with a cable routed in a general manner. When the

⋆ Corresponding author

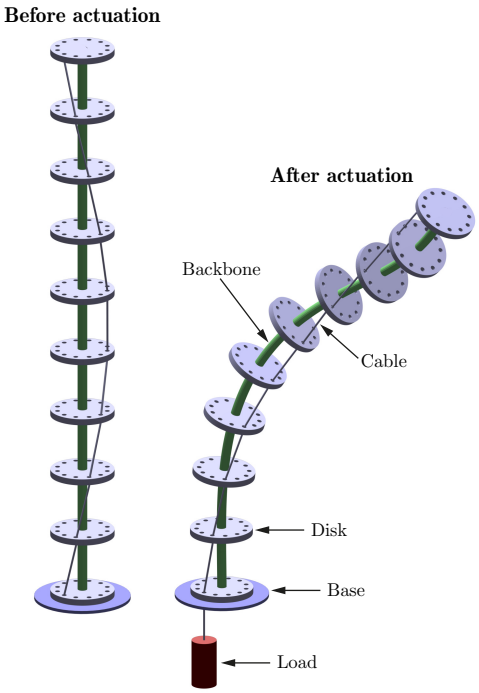

Fig. 1: Schematics of a CCR with a generally routed cable (a) before and (b) after actuation

cable is loaded (actuated) below the base, the entire CCR bends into a new shape that is determined by the routing of the cable. The resulting shape of the CCR (in Fig. 1a) after actuation is shown in Fig. 1b.

Various models to predict the shapes of a CCR can be found in the literature. A comprehensive review of such models can be found in [1,4,5,6]. Most of the available literature focuses on the straight routed CCR and sometimes with multiple sections. These models range from simple constant curvature approaches [7] to more detailed techniques such as finite element method (FEM) [8,9], Euler-Bernoulli beam theory along with statics [10,11], Cosserat rod theory [12,13] and pseudo-rigid body models [14] to mention a few. However, only a few models are available that can accurately model a generally routed CCR. Cosserat rod theory-based models have been shown to accurately model such CCR. Recently a geometry-based optimization method [15] has also shown to model such routing with good accuracy. Although studies have been performed on dexterity [16] and workspace [10] analysis on straight routed cables, it is still limiting as compared to the more complex shapes and positions a generally routed CCR can attain. It is thus necessary to develop an approach that can predict the routing of the cable to attain a desired shape of the backbone. In this paper, we propose one such

algorithm which can accomplish such a goal. We employ the optimization-based forward kinematics model [15] which is purely geometry-based and is shown to be accurate and faster [17] than models using the material parameters. We use the geometry-based approach to develop an algorithm that can provide the cable routing and the actuation details of a desired final shape of the CCR. By utilizing this algorithm, we aim to provide a tool for designing CCRs with complex shapes which can then exhibit more complex trajectories.

The rest of the paper is organized as follows: In section 2, a brief explanation of the optimization-based forward kinematics model along with the algorithm is discussed which is further validated in section 3. Finally, in section 4, concluding remarks and scopes of future work is discussed.

2 Methodology

In this section we present a brief description of the geometry-based optimization method as discussed in [15] and then describe the algorithm to obtain the cable routing for a CCR such that it can attain a desired shape on actuation.

2.1 Forwards kinematics of generally-routed CCR

The reference coordinate system is chosen to be at the base disk with the X-axis pointing towards the cable, Z-axis pointing vertically upwards and, the Y-axis obtained from the right-hand rule.

The disks are numbered 0 till n, starting from the base till the tip. In the undeformed state, the location of the center of i^{th} disk is given by $\mathbf{X}_0^i$. The hole through which the cable passes is at a distance a from $\mathbf{X}_0^i$ and it's location is given by $\mathbf{X}_a^i$. Please refer to the nomenclature presented at the end for more details[1].

Figure 2a shows the i^{th} section of the undeformed CCR. In this section, we consider two four bars (shown in red and green in Fig 2a). The first four bar consists of the vertices $\mathbf{X}_0^{i-1}$, $\mathbf{X}_a^{i-1}$, $\mathbf{X}_a^i$ and $\mathbf{X}_0^i$. The second four bar consists of vertices $\mathbf{X}_0^{i-1}$, $\bar{\mathbf{X}}_b^{i-1}$, $\bar{\mathbf{X}}_b^i$ and $\mathbf{X}_0^i$ (where $\bar{\mathbf{X}}_b^i$ is on the i^{th} disk and $\angle \mathbf{X}_a^i \mathbf{X}_0^i \bar{\mathbf{X}}_b^i = \pi/2$ rads). In these two imaginary four bars, $\mathbf{X}_0^{i-1}\mathbf{X}_a^{i-1}$ and $\mathbf{X}_0^{i-1}\bar{\mathbf{X}}_b^{i-1}$ are the fixed linkages, $\mathbf{X}_0^i\mathbf{X}_a^i$ and $\mathbf{X}_0^i\bar{\mathbf{X}}_b^i$ are the couplers and $\mathbf{X}_0^{i-1}\mathbf{X}_0^i$ being the first crank for both.

The geometry-based optimization algorithm is performed one section at a time starting from the base till the tip. After actuation, in the i^{th} section, the points $\mathbf{X}_0^i$, $\mathbf{X}_a^i$ and $\bar{\mathbf{X}}_b^i$ attains a new location given by, $\mathbf{x}_0^i$, $\mathbf{x}_a^i$ and $\bar{\mathbf{x}}_b^i$ which changes the four bars as seen in Fig. 2b. The optimization, to obtain the pose of the CCR, involves minimizing the coupler angle. It is mathematically given as:

$$\underset{\mathbf{x}_0^i, \mathbf{x}_a^i}{\arg\min} \quad \left(\left[\arccos\left(\frac{\mathbf{A}}{\|\mathbf{A}\|} \cdot \frac{\mathbf{B}}{\|\mathbf{B}\|} \right) \right]^2 + \left[\arccos\left(\frac{\mathbf{C}}{\|\mathbf{C}\|} \cdot \frac{\mathbf{D}}{\|\mathbf{D}\|} \right) \right]^2 \right) \tag{1}$$

[1] Note that the superscripts represent the disk number and not exponents

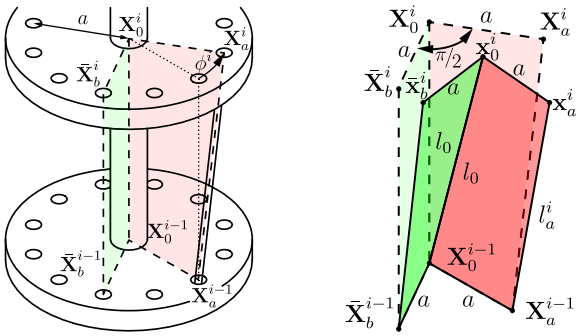

Fig. 2: Nomenclature used for (a) i^{th} undeformed section (b) two four-bars before (lightly shaded) and after actuation (shaded dark).

where, $\mathbf{A} = \mathbf{X}_0^{i-1} - \mathbf{X}_a^{i-1}$, $\mathbf{B} = \mathbf{x}_0^i - \mathbf{x}_a^i$, $\mathbf{C} = \mathbf{X}_0^{i-1} - \bar{\mathbf{X}}_b^{i-1}$, $\mathbf{D} = \mathbf{x}_0^i - \bar{\mathbf{x}}_b^i$

Subject to:

$$\begin{gathered} \left\|\mathbf{x}_0^i - \mathbf{X}_0^{i-1}\right\| = l_0, \quad \left\|\mathbf{x}_a^i - \mathbf{X}_a^{i-1}\right\| = l_a^i, \quad \left\|\mathbf{x}_0^i - \mathbf{x}_a^i\right\| = a, \\ \bar{\mathbf{X}}_b^i = a\,\frac{\left(\mathbf{X}_a^i - \mathbf{X}_0^i\right) \times \left(\mathbf{X}_0^i - \mathbf{X}_0^{i-1}\right)}{\left\|\left(\mathbf{X}_a^i - \mathbf{X}_0^i\right) \times \left(\mathbf{X}_0^i - \mathbf{X}_0^{i-1}\right)\right\|} \end{gathered} \tag{2}$$

Given data: $\mathbf{X}_0^i$, $\mathbf{X}_0^{i-1}$, $\mathbf{X}_a^i$, $\mathbf{X}_a^{i-1}$, l_0, l_a^i and a.

The solutions to this section, $\mathbf{x}_0^i$ and $\mathbf{x}_a^i$ are then used as the base linkage points for four bars in the next section – see [15,17] for more details.

The above optimization problem can be made as a function whose inputs are ϕ^i, a, l_0, l_a^i, $\mathbf{X}_0^{i-1}$, $\mathbf{X}_a^{i-1}$ and $\mathbf{X}_0^i$. The outputs to this function are $\mathbf{x}_0^i$ and $\mathbf{x}_a^i$. Symbolically this function is represented as f_{FK}.

2.2 Algorithm to obtain routing of cable

To determine the routing of the cable, when the desired shape is given, we first need to obtain the positions of the disks in the actuated position. If the desired shape is given as a curve, first we need to suitably modify the curve such that the starting point is $[0, 0, 0]^T$. We also need to decide the distance between two consecutive disks, l_0. This length should be such that each section doesn't have a large variation of slope and curvature. Additionally, we set a distance a, the distance of the cable from the disk's center. The desired disk locations can then be obtained by iteratively finding the intersection points between the given curve and a sphere of radius l_0, starting from the base of the CCR and progressing towards the tip. We denote these desired positions of the backbone as $\mathbf{x}_{0d}^i$.

In the algorithm to find the routing, the forward kinematics function f_{FK} as mentioned in the previous section is used to minimize e, the error between the output and the desired shape. This can be mathematically stated as:

$$\min_{\phi^i} \quad e \;=\; \left\|\mathbf{x}_0^i - \mathbf{x}_{0d}^i\right\| \tag{3}$$

where $\mathbf{x}_0^i = f_{\text{FK}}\left(\phi^i, a, l_0, l_a^i, \mathbf{X}_0^{i-1}, \mathbf{X}_a^{i-1}, \mathbf{X}_0^i\right)$ – the output $\mathbf{x}_a^i$ is ignored here.
Subject to:

$$-\pi/4 \;\leq\; \phi^i \;\leq\; \pi/4 \tag{4}$$

Given data: l_0, l_a^i, a, $\mathbf{X}_0^{i-1}$, $\mathbf{X}_a^{i-1}$ and $\mathbf{X}_0^i$

It may be noted that $\mathbf{X}_0^{i-1}$, $\mathbf{X}_a^{i-1}$ are the outputs of the previous iteration (or the positions on base disk for 1st iteration). For the first iteration, $\mathbf{X}_0^i = [0, 0, l_0]^T$ and for the rest,

$$\mathbf{X}_0^i = \mathbf{X}_0^{i-1} + \; l_0 \, \frac{\mathbf{X}_0^{i-1} - \mathbf{X}_0^{i-2}}{\left\|\mathbf{X}_0^{i-1} - \mathbf{X}_0^{i-2}\right\|}$$

Usually, ϕ^i is kept low as implemented in the constraint equation (4). This makes sure that the cable does not collide with the backbone. The quantity l_a^i can be obtained from geometry as:

$$l_a^i \;=\; \delta \sqrt{l_0^2 + 2a^2 - 2a^2 \cos\left(\phi^i\right)}$$

where, δ is the ratio of the cable inside the CCR after and before actuation.

Similar to the forward kinematics model, the optimization problem in equation (3) is solved one section at a time starting from the base till the tip, taking the solutions of the previous section as the base for the next section.

Once ϕ^i is obtained from the optimization problem (given by equation (3)), $\mathbf{X}_a^i$ can be obtained from geometry.

3 Results and discussions

3.1 Numerical simulations

For the purpose of validation, multiple cases were tried out, of which three cases are discussed here. The desired coordinates of the final shape for the cases are listed in Table 1. Values for all the parameters were chosen as: $n = 9$, $a = 8$ mm, $l_0 = 20$ mm. To solve the optimization problem given by equations (3) – (4), `fmincon` function in MATLAB® was used. *Interior-point algorithm* – an inbuilt algorithm in `fmincon` – is used and it takes an average of 23 seconds to simulate in a PC with a processor clocked at 3.1 GHz with 16 GB RAM. The inequality constraint (4) is implemented as upper and lower bounds on the optimization variables in `fmincon`.

For the first section, ϕ^i is taken as 0 degrees – this can be achieved by suitably rotating the whole curve about the Z-axis. While simulating, for the first section, δ is also kept as an optimization variable and the same value is used for the rest of the iterations. Initial guesses for $i = 1$ were chosen as $\phi = \pi/6$ rads and $\delta = 0.6$ (chosen arbitrarily). For the subsequent sections, the result (ϕ^i) of the previous iteration was provided as the initial guess.

Table 1: Details of the various cases along with the results.
(DC = Desired coordinates, e_{R} = RMS error (in mm))

Disk	**Case I**				**Case II**				**Case III**			
No.	DC (in mm)			ϕ	DC (in mm)			ϕ	DC (in mm)			ϕ
(i)	x	y	z	(deg)	x	y	z	(deg)	x	y	z	(deg)
0	0.00	0.00	0.00	0.00	0.00	0.00	0.00	0.00	0.00	0.00	0.00	0.00
1	2.54	-0.24	19.84	30.00	2.20	0.20	19.88	-30.00	1.89	0.06	19.91	-20.01
2	7.64	0.88	39.14	29.99	6.60	-0.78	39.36	-30.00	5.70	-0.58	39.53	3.36
3	14.20	4.46	57.69	30.03	12.32	-3.77	58.29	-13.10	11.15	-2.37	58.69	3.92
4	20.75	10.88	75.47	30.00	17.73	-9.64	76.63	-13.19	17.99	-5.39	77.24	3.90
5	25.54	20.03	92.59	-0.54	22.81	-17.86	94.14	-26.95	26.48	-9.20	94.95	-29.73
6	28.69	31.38	108.76	-3.25	27.47	-28.28	110.56	-27.04	36.72	-13.26	111.63	-29.53
7	30.12	44.68	123.63	-3.25	31.51	-40.53	125.85	29.11	48.65	-17.21	127.20	-11.33
8	29.81	59.65	136.88	-3.25	36.19	-54.50	139.38	22.78	62.12	-20.83	141.53	-19.25
9	27.75	75.98	148.25	-3.38	42.53	-69.34	151.19	5.83	76.99	-24.23	154.47	6.14
e_{R}	0.64				2.41				3.56			
δ	0.94				0.95				0.96			

3.2 Results

The numerical results for the cases listed in Table 1, were simulated using the forward kinematics model (section 2.1) to get the final shape of the CCR when actuated. The corresponding RMS value of error at each disk (e_{R}) is presented in Table 1. The corresponding plots are presented in Figure 3. As seen from the figures, the simulated shape closely follows the desired shape with a maximum RMS error of 3.56 mm, which is about 2% of the total length of the CCR. It should be noted that the same shape can be attained by other routing and amount of cable actuation. This algorithm produces only one of those results.

As mentioned, the final desired shape needs to be smooth and continuous. Additionally, the limitation of this algorithm includes the inability to modelling of gravity effect, which may be significant in the case of large CCR. The friction effects are also ignored in the modelling. Finally, the backbone cannot be very flexible as in that case the material properties and non-linearities will start to play a major role.

4 Conclusion

This paper presents a novel algorithm to obtain the routing of a generally-routed CCR for achieving a prescribed final shape. The algorithm utilizes a geometry-based optimization method for the forward kinematics model. The simulated result attains the desired shape with RMS error of less than 2% of the total length

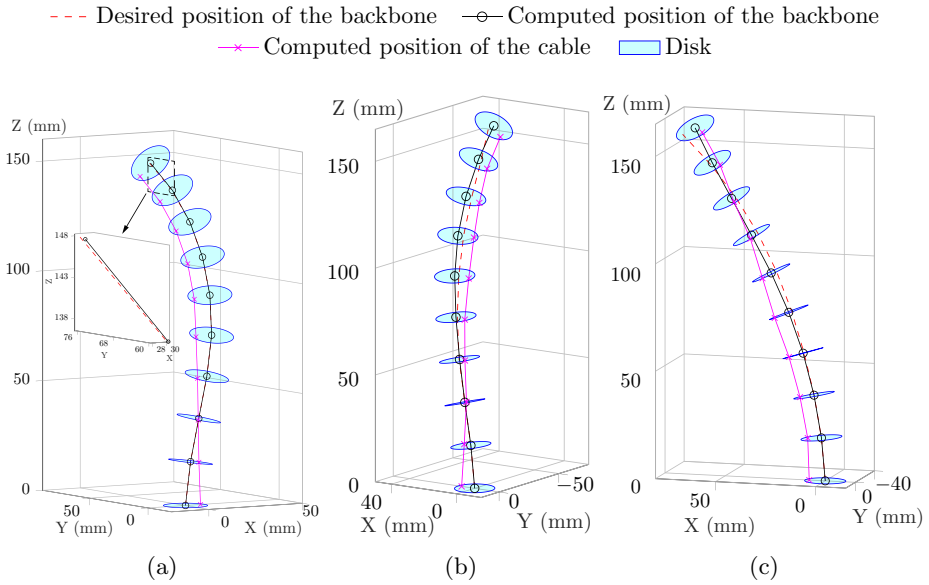

Fig. 3: Comparison of the desired and actual backbone positions for (a) Case I, (b) Case II and (c) Case III

of the backbone. The advantage of this method is that it is purely geometry-based, eliminating the need for material properties. Additionally, the information about the actuation – the amount of cable pull – is easier to visualize (or measure) than the applied force traditionally used. This algorithm makes designing a CCR that can achieve complex desired shapes and positions significantly easier.

Although this algorithm works well for the presented cases, a CCR cannot reach all possible curves in 3D. Identification of the feasible curves is a work in progress, along with the improvement of the algorithm with the implementation of better initial conditions based on the shape of the curve. Addition of variation of the distance of the cable from the center of the disk (variable a) and use of multiple cables will also expand the feasibility of obtaining more complex shapes and curves.

Nomenclature

References

1. Webster, R.J., Jones, B.A.: Design and kinematic modeling of constant curvature continuum robots: A review. The International Journal of Robotics Research **29**(13), 1661–1683 (2010)
2. Dupont, P.E., Simaan, N., Choset, H., Rucker, C.: Continuum robots for medical interventions. Proceedings of the IEEE **110**(7), 847–870 (2022)

Table 2: Nomenclatures used in the formulation

Symbol	Description
n	Number of backbone segments.
a	Distance between the disk's center and the hole with the cable.
l_0	Length of a backbone segment.
l_a^i	Length of the cable inside i^{th} segment.
δ	Ratio of the total length of the cable inside the CCR after and before actuation.
ϕ^i	Angular position of the cable in the i^{th} disk with respect to $(i-1)^{\text{th}}$ disk.
$\mathbf{X}_0^i$	Position vector of backbone at the i^{th} disk in undeformed state.
$\mathbf{X}_a^i$	Position vector of the cable at the i^{th} disk in unactuated state.
$\mathbf{x}_0^i$	Position vector of the deformed backbone at the i^{th} disk.
$\mathbf{x}_a^i$	Position vector of the cable at the i^{th} disk after actuation.
f_{FK}	Forward kinematics model as a function with inputs – $\left(\phi^i, a, l_0, l_a^i, \mathbf{X}_0^{i-1}, \mathbf{X}_a^{i-1}, \mathbf{X}_0^i\right)$, and outputs – $\left(\mathbf{x}_0^i, \mathbf{x}_a^i\right)$.
$\mathbf{x}_{0d}$	Positions of the centers of the disks of the CCR along the desired curve.

3. Russo, M., Sadati, S.M.H., Dong, X., Mohammad, A., Walker, I.D., Bergeles, C., Xu, K., Axinte, D.A.: Continuum robots: An overview. Advanced Intelligent Systems **5**(5), 2200,367 (2023)
4. Chirikjian, G.: Conformational modeling of continuum structures in robotics and structural biology: A review. Advanced Robotics **29**(13), 817–829 (2015)
5. Rao, P., Peyron, Q., Lilge, S., Burgner-Kahrs, J.: How to model tendon-driven continuum robots and benchmark modelling performance. Frontiers in Robotics and AI **7** (2021)
6. Armanini, C., Boyer, F., Mathew, A.T., Duriez, C., Renda, F.: Soft robots modeling: A structured overview. IEEE Transactions on Robotics **39**(3), 1728–1748 (2023)
7. Gravagne, I., Walker, I.: On the kinematics of remotely-actuated continuum robots. In: Proceedings 2000 ICRA. Millennium Conference. IEEE International Conference on Robotics and Automation. Symposia Proceedings (Cat. No.00CH37065), vol. 3, pp. 2544–2550. IEEE (2000)
8. Morales Bieze, T., Kruszewski, A., Carrez, B., Duriez, C.: Design, implementation, and control of a deformable manipulator robot based on a compliant spine. The International Journal of Robotics Research **39**(14), 1604–1619 (2020)
9. Grazioso, S., Di Gironimo, G., Siciliano, B.: A geometrically exact model for soft continuum robots: The finite element deformation space formulation. Soft Robotics **6**(6), 790–811 (2019)
10. Yuan, H., Li, Z.: Workspace analysis of cable-driven continuum manipulators based on static model. Robotics and Computer-Integrated Manufacturing **49**, 240–252 (2018)
11. Yuan, H., Zhou, L., Xu, W.: A comprehensive static model of cable-driven multi-section continuum robots considering friction effect. Mechanism and Machine Theory **135**, 130–149 (2019)

12. Rucker, D.C., Webster III, R.J.: Statics and dynamics of continuum robots with general tendon routing and external loading. IEEE Transactions on Robotics **27**(6), 1033–1044 (2011)
13. Till, J., Aloi, V., Rucker, C.: Real-time dynamics of soft and continuum robots based on cosserat rod models. The International Journal of Robotics Research **38**(6), 723–746 (2019)
14. Venkiteswaran, V.K., Sikorski, J., Misra, S.: Shape and contact force estimation of continuum manipulators using pseudo rigid body models. Mechanism and Machine Theory **139**, 34–45 (2019)
15. Ashwin, K.P., Ghosal, A.: Profile estimation of a cable-driven continuum robot with general cable routing. In: Advances in Mechanism and Machine Science, pp. 1879–1888. Springer International Publishing (2019)
16. Wang, J., Lau, H.Y.K.: Dexterity analysis based on jacobian and performance optimization for multi-segment continuum robots. Journal of Mechanisms and Robotics **13**(6) (2021). : 061012
17. Mahapatra, S.K., Ashwin, K.P., Ghosal, A.: Modelling of cable-driven continuum robots with general cable routing: a comparison. In: Advances in Asian Mechanism and Machine Science, pp. 345–353. Springer International Publishing (2022)